Published in final edited form as:

Nature. 2016 September 29; 537(7622): 634–638. doi:10.1038/nature19331.

SEDS proteins are a widespread family of bacterial cell wall polymerases

Alexander J. Meeske[1], **Eammon P. Riley**[1], **William P. Robins**[1], **Tsuyoshi Uehara**[1], **John J. Mekelanos**[1], **Daniel Kahne**[2,3], **Suzanne Walker**[1,2,3], **Andrew C. Kruse**[2], **Thomas G. Bernhardt**[1,*], and **David Z. Rudner**[1,*]

[1]Department of Microbiology and Immunobiology, Harvard Medical School, 77 Avenue Louis Pasteur, Boston MA 02115

[2]Department of Biological Chemistry and Molecular Pharmacology, Harvard Medical School, 250 Longwood Ave, Boston, MA 02115, USA

[3]Department of Chemistry and Chemical Biology, Harvard University, Cambridge, MA, 02138, USA

Summary

Elongation of rod-shaped bacteria is mediated by a dynamic peptidoglycan synthetic machinery called the Rod complex. We report that in *Bacillus subtilis* this complex is functional in the absence of all known peptidoglycan polymerases. Cells lacking these enzymes survive by inducing an envelope stress response that increases expression of RodA, a widely conserved core component of the Rod complex. RodA is a member of the SEDS family of proteins that play essential but ill-defined roles in cell wall biogenesis during growth, division and sporulation. Our genetic and biochemical analyses indicate that SEDS proteins constitute a new family of peptidoglycan polymerases. Thus, *B. subtilis* and likely most bacteria use two distinct classes of polymerases to synthesize their exoskeleton. Our findings indicate that SEDS family proteins are core cell wall synthases of the cell elongation and division machinery, and represent attractive targets for antibiotic development.

Text

The peptidoglycan (PG) cell wall is the bacterial exoskeleton. It specifies cell shape, protects the cell from osmotic lysis, and its biogenesis is among the most enduring targets for therapeutic intervention. PG is composed of polysaccharide chains crosslinked to each other

*Correspondence and requests for materials should be addressed to: rudner@hms.harvard.edu and thomas@hms.harvard.edu.

Supplementary Information is linked to the online version of the paper at www.nature.com/nature.

Author Contributions: The project was conceived by AJM, TU, TGB, and DZR. Experiments were carried out by AJM and EPR. MutSeq library preparation and analysis were performed by EPR and WPR with assistance from JJM. ACK assisted in protein purification. DK and SW provided synthetic lipid II and moenomycin. The manuscript was written by AJM, TGB, and DZR.

The authors declare no competing financial interests.

by short peptides. This meshwork is synthesized by peptidoglycan glycosyltransferases (PGT) that polymerize the glycan strands from a lipid-linked precursor called lipid II. The nascent strands are incorporated into the existing meshwork by the transpeptidase (TP) activity of penicillin binding proteins (PBPs), which crosslink stem peptides attached to the polysaccharide chains. Glycan strand synthesis is carried out by a subset of PBPs called Class A PBPs (for simplicity, referred to as aPBPs) that are bi-functional enzymes possessing a glycosyltransferase 51 (GT51) domain and a TP domain[1,2]. aPBPs are thought to polymerize glycan strands in the context of two essential and broadly conserved cell wall synthetic machines. The Rod complex (also called the elongasome) polymerizes PG along the cell cylinder to drive cell elongation, while the divisome synthesizes PG during cytokinesis generating the incipient cell poles[3].

Intriguingly, a small subset of bacteria that possess PG lack aPBPs and do not encode other proteins with GT51 domains[4]. Furthermore, the model Gram-positive bacterium *Bacillus subtilis* encodes four aPBPs, yet Popham and co-workers reported over a decade ago that cells lacking all four enzymes are viable, make PG, and are rod-shaped (Fig. 1a)[5]. Similar findings have been made in two species of *Enterococcus*[6,7]. Under these conditions, cross-linking of adjacent glycan strands is likely carried out by the essential Class B PBPs (for simplicity, bPBPs), which have TP domains but lack PGT activity[1]. However, the enzyme(s) responsible for polymerizing the glycan strands in these cells is completely unknown. It is also unclear whether these unidentified PGTs are central players in cell wall synthesis or moonlighting enzymes that compensate for the loss of aPBP function[5].

The Rod complex functions without aPBPs

To investigate whether the cell wall elongation machinery is functional in the absence of the aPBPs, we monitored a GFP-labeled component (Mbl) of the Rod complex by time-lapse fluorescence microscopy. Recent work indicates that the Rod complex moves in a directed and circumferential manner around the long axis of the cell[8–10]. This movement depends on active cell wall synthesis, and thus reflects Rod complex-dependent PG polymerization. Strikingly, cells lacking all four aPBPs exhibited GFP-Mbl dynamics that were qualitatively and quantitatively similar to wild-type (Fig. 1b–e and Supplementary Videos 1 and 2). Furthermore, the directed movement was sensitive to the cell wall synthesis inhibitors vancomycin and ampicillin (Fig. 1f, Extended Data Fig. 1a–b, Supplementary Videos 3–4). Thus, Rod complex-dependent PG synthesis is largely unaffected in the absence of all known PGTs. Consistent with these findings, GFP-Mbl dynamics in wild-type cells were unperturbed by moenomycin, an inhibitor of the glycosyltransferase activity of aPBPs (Extended Data Fig. 1c–d, Supplementary Video 5). We conclude that an unidentified PGT provides the critical polymerase activity needed for Rod complex function. Furthermore, since cells lacking the aPBPs are capable of dividing[5] (Fig. 1a), the same or a related PGT activity is also likely to function in the divisome.

SEDS proteins bear similarity to known GTs

We reasoned that either a single unidentified synthase acts in both the Rod complex and the divisome, or there are two homologous enzymes, one for each complex. In line with the

latter hypothesis, two protein families are represented in both synthetic machines: the bPBPs which crosslink the stem peptides on the glycan strands and the SEDS (Shape, Elongation, Division and Sporulation) family of enigmatic function[11]. The bPBPs and SEDS proteins are thought to work together as a subcomplex[12–15], and are genetically linked in many bacteria (Extended Data Fig. 2). In *B. subtilis*, the bPBP-SEDS pair present in the Rod complex is PBP2A (or PBPH) and RodA, respectively[16,17], while PBP2B and FtsW are components of the divisome[18,19]. Intriguingly, three decades ago Ishino and co-workers provided evidence that members of these two families stimulate PGT activity in *Escherichia coli*[20] but these findings were never extended or corroborated.

Using the remote homology detection algorithm HHpred[21], we discovered that the SEDS proteins exhibit weak similarity to O-antigen ligases involved in synthesis of lipopolysaccharide (LPS) in Gram-negative bacteria. Although the homology did not extend to conserved sequence motifs, the secondary structure and positional amino acid distribution produced a high confidence match (Probability 98.4%, E-value 0.0071). O-antigen ligase is a polytopic membrane protein glycosyltransferase that carries out the *en bloc* transfer of undecaprenyl-pyrophosphate-linked O-antigen polymers to a Lipid A-core glycolipid acceptor (Fig. 2)[22]. Like the SEDS proteins, O-antigen ligases contain 10–12 transmembrane segments and a large extracytoplasmic loop that is required for activity. Moreover, peptidoglycan precursors are similarly linked to an undecaprenyl-pyrophosphate carrier (Fig. 2). O-antigen ligase represents one of many multipass membrane protein glycosyltransferases that use lipid-linked precursor substrates, including proteins involved in the synthesis of LPS and other surface polymers, as well as O- and N-linked protein glycosylation (Fig. 2)[22–26]. On the basis of these observations, we hypothesized that the SEDS proteins RodA and FtsW are the unidentified PGTs in the Rod complex and the divisome, respectively.

RodA expression suppresses the aPBP mutant

To investigate whether RodA can catalyze PGT activity, we sought to purify RodA from the *B. subtilis* strain lacking all four aPBPs (Δ4) to avoid contaminating activities. A functional *rodA-his*$_{10}$ fusion under the control of a strong IPTG-inducible promoter was introduced into the quadruple aPBP mutant. Strikingly, we discovered that ~10-fold over-production of RodA-His10 significantly alleviated the growth defect of the quadruple mutant (Fig. 3a and Extended Data Fig. 3a,d). Furthermore, examination of these cells by fluorescence microscopy revealed nearly complete suppression of the cell width and elevated lysis phenotypes observed in the Δ4 mutant (Fig. 3b–c, and Extended Data Fig. 3b–c).

Isolated membranes from wild-type cells, the Δ4 mutant, and the Δ4 mutant overexpressing RodA-His10 were assayed for PGT activity using radiolabeled synthetic lipid II[27]. As expected, membranes lacking the aPBPs had less activity than WT (Fig. 3d). However, PGT activity was significantly higher in the membranes in which RodA was over-produced. Furthermore, RodA and RodA-dependent PGT activity could be solubilized by the zwitterionic detergent CHAPS (Fig. 3d and Extended Data Fig. 3e). These experiments suggest that RodA is a PGT or stimulates an unidentified PGT. However, despite substantial effort, we were unable to affinity purify RodA-His10 under these conditions.

RodA has PGT activity *in vitro*

To improve RodA purification, we constructed an *E. coli* expression system modeled after those used to purify G protein-coupled receptors, in which a SUMO-FLAG-RodA fusion and the SUMO protease Ulp1 were co-expressed. SUMO cleavage generates an amino-terminal aspartic acid in the FLAG tag that is recognized by the M1 anti-FLAG monoclonal antibody allowing for rapid and specific immuno-affinity purification. To reduce possible contamination from *E. coli* aPBPs and other proteins containing GT51 domains, we deleted three (*ponB*, *pbpC*, *mtgA*) of the four genes that encode them from our expression strain. The only remaining family member was PBP1A, whose presence during RodA purification could be tracked by immunoblot. FLAG-RodA was immunopurified from detergent-solubilized membranes and eluted with EDTA and FLAG peptide. The protein, estimated to be 60% pure (Fig. 4a), catalyzed the conversion of lipid II into glycan chains *in vitro* (Fig. 4b–c and Extended Data Fig. 4). Importantly, the PGT activity was resistant to moenomcyin at concentrations that inhibit PBP1A[28] as well as SgtB, a PGT from *Staphylococcus aureus* (Fig. 4b–c), suggesting the activity was not due to aPBP contamination. To test whether RodA was responsible for glycan strand polymerization, we sought to assay non-functional mutants. We screened for essential residues in RodA by mutagenesis followed by high-throughput sequencing (MutSeq)[29]. Among the residues identified in our screen (Supplementary Table 1 and Extended Data Fig. 5a), we chose two (W105 and D280) predicted to be in the second and fourth extracellular loops of RodA (Extended Data Fig. 5). Alanine substitutions at either position abolished RodA function *in vivo* without affecting protein levels (Fig. 3a and Extended Data Fig. 6). Purified FLAG-RodA(W105A) and separately (D280A) (Fig. 4a) failed to polymerize glycan strands (Fig. 4b–c). Importantly, immunoblot and mass spectrometry analyses indicate that the levels of PBP1A and other *E. coli* contaminating proteins were similar in all three purifications (Fig. 4a and Supplementary Table 2). Although we cannot formally rule out the possibility that a novel moenomycin-resistant *E. coli* PGT that is present in our purified preparation is stimulated by wild-type RodA but not by either point mutant, our data are most consistent with the conclusion that RodA is a PG polymerase.

RodA induction confers moenomycin resistance

B. subtilis is intrinsically resistant to moenomycin, and this resistance is dependent upon the extracytoplasmic function (ECF) sigma factor SigM (σ^M)[30] (Fig. 4d). Consistent with the idea that aPBPs are specifically targeted by moenomycin, we found that cells lacking all four aPBPs require *sigM* for viability (Fig. 4e). Among the genes that are induced by σ^M in response to envelope stress is *rodA*[31]. In light of our data that RodA is a moenomycin-resistant PGT (Fig. 4b–c), we investigated whether *rodA* upregulation was responsible for this natural resistance. Indeed, overexpression of *rodA* restored moenomycin resistance to a *sigM* null mutant (Fig. 4d). Furthermore, it suppressed the synthetic lethality of the Δ*sigM* Δ4 aPBP mutant (Extended Data Fig. 7a). To directly test whether σ^M-dependent expression of *rodA* provides moenomycin resistance, we mutated the σ^M recognition sequences (both −10 and −35 elements) in the *rodA* promoter. In the absence of drug, the promoter mutant ($P_{\Delta sigM}$) was indistinguishable from wild-type with respect to growth rate and morphology (Extended Data Fig. 7b–c). However, the $P_{\Delta sigM}$ mutant was sensitive to moenomycin and synthetically lethal with the quadruple aPBP deletion (Fig. 4d–e). Thus, increased

expression of *rodA* mediated by σ^M is both necessary and sufficient to confer intrinsic resistance to moenomycin and viability to cells lacking the aPBPs.

Discussion

Here, we have presented evidence that the SEDS family protein RodA is the principal PGT in the Rod complex and is likely to be responsible for its dynamic movement. Since *B. subtilis* cells lacking all aPBPs undergo cytokinesis, by extension, we propose that the SEDS family protein FtsW plays a similar role in the divisome. The requirement of SEDS proteins for cell wall biogenesis; the extensive genetic linkage between the genes encoding SEDS proteins and those involved in PG synthesis (Extended Data Fig. 2); and the nearly universal conservation of the residues essential for the catalytic activity of RodA (Extended Data Fig. 5b) collectively argue that SEDS proteins constitute a widespread family of peptidoglycan glycosyltransferases. Furthermore, given that SEDS and bPBPs are known to interact, these factors likely function together within their designated complexes as cognate enzyme pairs that polymerize and crosslink nascent PG into the existing meshwork.

Phylogenetic analysis indicates that SEDS family members and bPBPs are more broadly conserved than aPBPs (Extended Data Fig. 8). In particular, a subset of bacteria including the pathogens *Francisella tularensis* and *Chlamydia trachomatis*, possess a cell wall but do not encode aPBPs. Among these taxa are organisms recently discovered to make PG[32–35] or encode an essential lipid II biosynthetic pathway[36]. In all cases, these organisms contain at least one SEDS family member and a bPBP, and we hypothesize that the assembly of their cell wall is mediated by these enzymes. Based on these and previous findings[20], we propose that SEDS-bPBP pairs are the core PG synthases in the cell wall elongation and division machineries. The specific role(s) of the aPBPs and whether or not they function in the context of these complexes remain important questions for future investigation. SEDS family members have previously been proposed to transport PG precursors (lipid II) across the cytoplasmic membrane, however, recent evidence suggests that they are not required for this process and that MurJ family members likely fulfill this role[37,38]. While it is formally possible that SEDS proteins are both PG polymerases and lipid II flippases, we favor the idea that these activities are catalyzed by distinct families of proteins. This view is informed by spore formation in *B. subtilis*, where a thick layer of spore-specific cell wall called the cortex is deposited around the developing spore. No aPBP has been found to be required for cortex biogenesis[39]. However, there are three sporulation-induced proteins that are absolutely essential: a MurJ homolog (SpoVB); a SEDS family member (SpoVE); and a bPBP (SpoVD)[40]. These three protein families possess the three activities (flippase, PGT, TP) required to build a cell wall, and thus may constitute a minimal PG assembly machine. Finally, drugs that target cell wall synthesis are among the most effective in combatting bacterial infection. The discovery that SEDS family proteins are PGTs with extracytoplasmic catalytic centers provides an attractive new avenue to target this pathway for antibiotic development.

Methods

General methods

B. subtilis strains were derived from the prototrophic strain PY79. Unless otherwise indicated, cells were grown in LB or CH medium at 37° C. Insertion-deletion mutants came from the *B. subtilis* knock out collection (back-crossed to PY79) or were generated by isothermal assembly[41] of PCR products followed by direct transformation into *B. subtilis* PY79. Antibiotic cassette removal was performed using a temperature-sensitive plasmid encoding Cre recombinase as described previously[38]. Moenomycin was purified from flavomycin feed stock as previously described[42]. For RodA-mediated suppression of the quadruple aPBP strain, *rodA* was induced with 50 μM IPTG. For all other induction experiments IPTG was used at 500 μM. Lists of strains (Supplementary Table 3), plasmids (Supplementary Table 4) and oligonucleotide primers (Supplementary Table 5) can be found online as supplementary information. A description of strain and plasmid construction can be found below. Source data for all SDS-PAGE experiments can be found in Supplementary Fig. 1.

Immunoblotting

SDS-PAGE lysates were prepared by brief lysozyme treatment and resuspension in an equal volume of 2X Laemmli buffer. Generally, 2–10 mOD units were loaded for analysis on 15% SDS-PAGE gels. For analysis of membrane proteins, samples were not heated prior to electrophoretic separation. Proteins were transferred to a methanol-activated PVDF membrane, blocked with 5% milk, probed with anti-His (Genscript, 1:4,000), anti-σ^A (1:10,000)[43], anti-ParB (1:5,000)[44] primary antibody, then horseradish peroxidase-coupled anti-rabbit (Bio-Rad) or anti-mouse (Bio-Rad) secondary antibody. Proteins were detected using Western Lightning chemiluminescence reagent.

Fluorescence microscopy

Exponentially growing cells were concentrated by centrifugation at 8,000 rpm for 1 min and immobilized on 1% agarose pads containing growth medium. Fluorescence microscopy was performed using an Olympus BX61 microscope equipped with a UplanF1 100X phase contrast objective lens and a CoolSnapHQ digital camera (Photometrics) or a Nikon Ti-E inverted microscope with a Nikon CFI Plan Apo VC 100X objective lens. Images were acquired using Metamorph or Nikon Elements software. Membranes were stained with TMA-DPH (50 μM) (Molecular Probes). Live-dead staining was performed with propidium iodide (5 μM) (Invitrogen). GFP-Mbl images were acquired using an ND8 neutral density filter to limit phototoxicity and photobleaching. For time-lapse imaging, images were acquired every 2 sec for 4 min. For vancomycin or ampicilllin addition experiments, drugs were added directly to the agarose pad containing the cells prior to imaging. Exposure times were 400 ms for TMA-DPH and propidium iodide, 500ms for GFP-Mbl. Image analysis and processing were performed in Fiji.

B. subtilis membrane preparation and detergent solubilization of membrane proteins

Membranes were isolated from 50 mL *B. subtilis* cultures grown in LB at 37°C. At OD600 = 0.4, IPTG was added to 500 μM to induce RodA-His10. After a 1 h induction, cells were pelleted by centrifugation and frozen at −80°C. The cell pellets were resuspended in 20 ml lysis buffer (50 mM HEPES pH 7.5, 0.3 M NaCl) and lysed by two passes at 20,000 psi in a French Pressure cell. Unbroken cells were removed by centrifugation at 4,000*g* for 10 min at 4°C. Membranes were collected by ultracentrifugation at 100,000*g* for 1 h at 4°C. The membrane pellet was dispersed in 1 ml 50 mM HEPES pH 7.5, 0.5 M NaCl, 20% glycerol at a protein concentration of 1 mg/ml. For detergent solubilization, CHAPS (Anatrace) was added to a final concentration of 2% and incubated overnight at 4°C. Solubilized membrane proteins were isolated by ultracentrifugation at 100,000*g* for 1 h at 4°C.

Protein purification

Protein expression was carried out in an *E. coli* C43 derivative of BL21 (DE3) harboring deletions in *ponB*, *pbpC*, *mtgA* (strain CAM333) carrying a plasmid-borne arabinose-inducible $Ulp1_{(403–621)}$ protease (pAM174). The SUMO-FLAG-RodA expression plasmid and mutant derivatives (pAM172, pAM172b, pAM172c) were transformed into the expression strain under selection for both plasmids. 5 fresh transformants from each were inoculated into 5 ml LB supplemented with ampicillin (50 μg/ml) and grown to exponential phase at 37°C and then diluted into 1 L LB + 50μg/ml ampicillin. Cultures were grown at 37°C to OD600 = 0.3 and shifted to 30°C. At OD600 = 0.6, IPTG was added (1 mM final) to induce RodA and arabinose was added (0.2% final) to induce Ulp1. After a 5 h induction, cells were pelleted and frozen at −80°C. Cell pellets were resuspended in lysis buffer (50mM HEPES pH 7.5, 0.3 M NaCl), lysed, and membranes isolated as described above. Membranes were mechanically homogenized using a teflon dounce, and solubilized in a mixed detergent system containing CHAPS (0.5%) and n-dodecyl-β-D-maltoside (DDM) (0.5%) for 90 min at 4°C. Insoluble material was removed by ultracentrifugation at 100,000*g* for 1 h at 4°C. The soluble fraction was supplemented with 2 mM $CaCl_2$ and applied to 1 mL M1 anti-FLAG antibody resin[45]. The resin was washed with 80 ml wash buffer (50 mM HEPES pH 7.5, 0.5 M NaCl, 20% glycerol, 2 mM $CaCl_2$, 0.05% DDM, 0.5% CHAPS). FLAG-RodA and mutants were eluted with 4 ml wash buffer supplemented with FLAG peptide (0.2 mg/mL) and 5 mM EDTA.

PGT activity assay

PGT activity in *B. subtilis* membranes, detergent-solubilized membrane proteins, and immuno-purified proteins from *E. coli* was assayed as previously described[27]. Briefly, membranes or protein samples were incubated with 4 μM ^{14}C-labeled synthetic lipid II with a heptaprenyl alkyl chain for 1 h unless otherwise indicated. The reaction buffer consisted of 20% DMSO, 50 mM HEPES pH 7.0, 20 mM $MgCl_2$, 20 mM $CaCl_2$. For *B. subtilis* membranes and detergent-solubilized membrane proteins, the final protein concentration was 0.05 mg/ml. Purified proteins were used at a final concentration of 0.2 μM. Moenomycin and mutanolysin (Sigma-Aldrich) were used at 0.6 μM and 100 μg/ml, respectively. Synthetic lipid II was synthesized as previously described[27]. Reactions were quenched by the addition of an equal volume of 10% Triton-X-100. Substrate and products

were resolved by paper chromatography. The reactions were spotted onto 20 cm paper strips and chromatography was carried out for 8 h using a mobile phase of isobutyric acid : 1M NH_4OH (5:3). Strips were cut 2.5 cm from the origin and each section was analyzed by scintillation counting (Ecolite scintillation cocktail). Counts at the origin-proximal section represent polymeric glycan products, while counts on the distal part of the strip represent unpolymerized lipid II (or short oligomers). For SDS-PAGE-based analysis, reaction products were quenched by boiling for 2 min, dried by speedvac and resuspended in 10 μl Laemmli buffer and resolved on a 20×20cm 12% polyacrylamide gel. The gel was dried and exposed to a phosphor screen for 2 weeks.

Mut-Seq library preparation and data analysis

Mut-seq was performed on two independently generated libraries, as previously described[29]. In brief, PCR mutagenesis of the *rodA* open reading frame was performed using GeneMorph II Random Mutagenesis Kit (Stratagene) under conditions yielding ~1.4 mut/kb with primers oDR1067 and oDR1068 and PY79 genomic DNA. A mutant library was constructed using isothermal assembly of PCR-mutagenized *rodA* with upstream and downstream homology regions and a spectinomycin resistance cassette generated by high-fidelity PCR (upstream region: primers oDR1069 and oDR1070 and PY79 genomic DNA; downstream region and spec(R) gene: oDR1071 and oDR1072 and BDR2702 genomic DNA). The assembled products were transformed directly into competent *Bacillus subtilis* PY79 selecting for Spec(R) and RodA function. >50,000 transformants were pooled, aliquoted, and frozen. Genomic DNA was extracted from each replicate and the *rodA* locus amplified by PCR (primers oDR1081 and oDR1082). PCR products were column purified and fragmented by sonication to an average size of 200 bp. Libraries were constructed using the NEBNext DNA Library Mastermix kit and amplified with primers for Illumina sequencing. 50 bp single-end sequencing was carried out on the Illumina HiSeq 2000 platform. Reads were mapped to the *B. subtilis* PY79 genome reference sequence (GenBank accession: CP006881) and filtered using CLC-Genomics Workbench software. Reads with a single mismatch were quality-filtered by applying a CASAVA 1.8 quality score filter of 38 or higher. On average, we detected 143,000 quality-filtered SNPs, corresponding to approximately 120 SNPs per nucleotide in the RodA coding sequence. The number of mutations at each nucleotide position and their corresponding amino acid changes were tabulated (Supplementary Table 1). Both G->T and C->A transversions were overrepresented when compared to all other classes of mutations and the average counts did not substantially differ between synonymous and nonsense mutations. These are among the most predominant rare mutations in deep-sequence DNA libraries and are thought to be generated by oxidative damage to DNA generated before and after DNA isolation by processes such as sonication-based shearing. We excluded these two mutation types from our analysis. The complete raw dataset is available on sheets 2–4 of Supplementary Table 1. For all other classes of nucleotide changes, the mean number of synonymous and nonsense mutations (when applicable) were used as thresholds to assess whether or not a missense mutation was permissive.

Strain construction

All deletion mutants except Δ*sigM* and *rodA* $P_{\Delta sigM}$ were generated by isothermal assembly followed by direct transformation into *B. subtilis*. All assembly reactions had three PCR products: an antibiotic resistance gene and upstream and downstream fragments that flank the locus to be deleted. A *loxP*-flanked kanamycin resistance cassette was amplified using oligonucleotide primers oJM28 and oJM29 and pWX470 as template. Upstream and downstream PCR products were amplified from PY79 genomic DNA using the following oligonucleotide primers: *pbpF* (oAM38, oAM39, oAM42, oAM43), *pbpG* (oAM44, oAM45, oAM48, oAM49), *pbpD* (oAM50, oAM51, oAM54, oAM55), *ponA* (oJM001, oJM002, oJM003, oJM004), *rodA* (oDR1069, oDR1124, oDR1125, oDR1072).

The Δ*sigM* deletion was derived from the *B. subtilis* knockout collection and was confirmed by PCR using oKO000 (within the erythromycin resistance cassette) and an upstream primer oKO82.

The *rodA* $P_{\Delta sigM}$ mutant was generated by allelic replacement using the pminiMAD-derived plasmid pAM199. This plasmid, harboring mutations in the −10 and −35 elements recognized by SigM[46] was transformed into PY79 selecting for resistance to erythromycin. Transformants were grown without selection at 22°C and plated on LB agar at 37°C. Single colonies were screened for loss of the integrated plasmid and sensitivity to erythromycin. Genomic DNA was prepared from four independent Erm(S) colonies and the *rodA* promoter region was PCR amplified and sequenced (using primer oAM201) to identify strains harboring the SigM promoter mutations.

E. coli expression strain CAM333 [C43 Δ*ponB* Δ*pbpC* Δ*mtgA* pP_{BAD}-*Ulp1*$_{(403–621)}$] was constructed by sequential P1 transduction and antibiotic cassette removal of the FRT-flanked *ponB::kan, pbpC::kan,* and *mtgA::kan* deletions from the Keio collection[47]. The kanamycin resistance cassettes were excised by expression of FLP recombinase from a temperature-sensitive plasmid at 30°C, and the plasmid was subsequently lost by nonselective growth at 37°C. All three deletions were confirmed by PCR using primers flanking the deleted gene (*ponB*: primers TB1290 and TB1291, *pbpC*: primers TB633 and TB644, *mtgA*: primers TB635 and TB636). The strain was then transformed with pAM174 [P_{BAD}-*Ulp1*$_{(403–621)}$ (cat) p15A *ori*].

Plasmid constructions

pAM84 [*amyE::*P*hyperspank-rodA-his10 (spec)(amp)*] was generated in a two-way ligation of a HindIII-NheI *rodA-his10* PCR product (amplified in sequential PCR steps with oligonucleotide primers oAM231 and oAM114 followed by oAM231 and oAM233 from PY79 genomic DNA) and pDR111 (*amyE::*P*hyperspank spec amp*) cut with HindIII and NheI.

pAM84b [*amyE::*P*hyperspank-rodA(W105A)-his10 (spec)(amp)*] was generated by site-directed mutagenesis from pAM84 using oDR1107

pAM84c [*amyE::*P*hyperspank-rodA(D280A)-his10 (spec)(amp)*] was generated by site-directed mutagenesis from pAM84 using oDR1104

pAM199 [*rodA* P*ΔsigM pminiMAD (erm) (amp)*] was generated in a three-way isothermal assembly reaction containing: *rodA* promoter fragment 1 (amplified from PY79 genomic DNA with oligonucleotide primers oAM517 and oAM518); *rodA* promoter fragment 2 (amplified from PY79 genomic DNA with oligonucleotide primers oAM519 and oAM520) and pminiMAD (*erm, amp*) digested with BamHI and HindIII. The σ^M-dependent *rodA* promoter (with −35 and −10 elements in bold) was changed from:

5′ TCAAT**CGAAAC**ATTTCGGTTTATGATA**CGTC**ATATTTCGT 3′ to

5′ TCAAT**CTGCGC**ATTTCGGTTTATGATA**TACT**ATATTTCGT 3′

pAM14 [*ycgO::*P*spank*-ponA (cat) (amp)*] was generated in a two-way ligation reaction with a PCR product containing *ponA* (amplified from PY79 genomic DNA using oligonucleotide primers oAM62 and oAM64) and pAM12 (*ycgO::*P*spank* cat amp*) digested with XmaI and SpeI.

pER135 [*ycgO::Pspank-rodA (erm) (amp)*] was generated in a two-way ligation reaction with a PCR product containing *rodA* (amplified from PY79 genomic DNA using oligonucleotide primers oDR1122 and oDR1123) and pER62 (*ycgO::*P*spank erm amp*) digested with HindIII and BamHI.

pER133 [*amyE::PxylA-rodA (spec) (amp)*] was generated in a two-way ligation reaction with a PCR product containing *rodA* (amplified from PY79 genomic DNA using oligonucleotide primers oDR1122 and oDR1123) and pDR150 (*amyE::*P*xylA spec amp*) digested with HindIII and BamHI.

pER155 [*amyE::PxylA-rodA (E288A) (spec) (amp)*] was generated by site-directed mutagenesis of pER133 using oDR1119.

pER146 [*amyE::Pxyl-rodA (D280A) (spec) (amp)*] was generated by site-directed mutagenesis of pER133 using oDR1104.

pER160 [*amyE::Pxyl-rodA (W105A) (spec) (amp)*] was generated by site-directed mutagenesis of pER133 using oDR1107.

pER157 [*amyE::PxylA-rodA (E117A) (spec) (amp)*] was generated by site-directed mutagenesis of pER133 using oDR1128.

pAM174 [P_{BAD}-*Ulp1*$_{(403–621)}$ *(cat)* p15A *ori*] was generated in a two-piece isothermal assembly reaction with a His6-Ulp1$_{(403–621)}$ PCR product (amplified from pTB145 (P_{T7}-*His6-Ulp1*$_{(403–621)}$) using oligonucleotide primers oAM453 and oAM454) and pMT30 (P_{BAD}-*sfgfp p15A cat*) digested with NdeI and HindIII.

pAM172 [P_{T7}-*His6-SUMO-FLAG-RodA (amp)*] was generated in a three-piece isothermal assembly reaction with FLAG-RodA fragment 1 (amplified from *FLAG-RodA* gBlock (IDT) using oligonucleotide primers oAM449 and oAM450), FLAG-RodA fragment 2 (amplified from PY79 genomic DNA using oAM446 and oAM447) and pTB146 (P_{T7}-*His6-SUMO amp*) digested with SapI and XhoI.

pAM172b [P$_{T7}$-*His6-SUMO-FLAG-RodA(W105A) (amp)*] was generated by site-directed mutagenesis of pAM172 using oDR1107.

pAM172c [P$_{T7}$-*His6-SUMO-FLAG-RodA(D280A) (amp)*] was generated by site-directed mutagenesis of pAM172 using oDR1104.

The sequence of the *FLAG-RodA* gBlock was:
ATGGAGAATCTGTATTTTCAGGACTACAAAGACGACGACGACCTGGAAGTTCTGT
TCCAGGGTCCGGGTGGTTCTTCTAGTCGATATAAGAAACAGCAAAGCCCCTTTTAC
CAGGGGGATTTGATTTTTATATTTGGTGTGTTTTTTATTATAAGCGTAGTATCAATAT
ATGCTGCCGGTCAGTTTGGGCAGTATGGGAACACGGATTGGATTCAGCAAATTGT
GTTTTATCTTTTGGGGGCTGTAGCCATTACAGTTCTTTTGTACTTTGATTTAGAACA
GCTTGAAAAGTTAAGTTTATATATTTTTATCATTGGTATTTTATCTTTGATTATTCTTA
AAATCAGTCCCGAGTCTATTGCACCTGTTATTAAAGGGGCAAAAAGTTGGTTTAG
GATCGGTAGAATAACAATACAGCCGTCAGAGTTTATGAAGGTTGGTTTGATTATGA
TGCTTGCTTCAGTTATTGGAAAAGCAAATCCTAAAGGAGTTCGGACGC

Extended Data

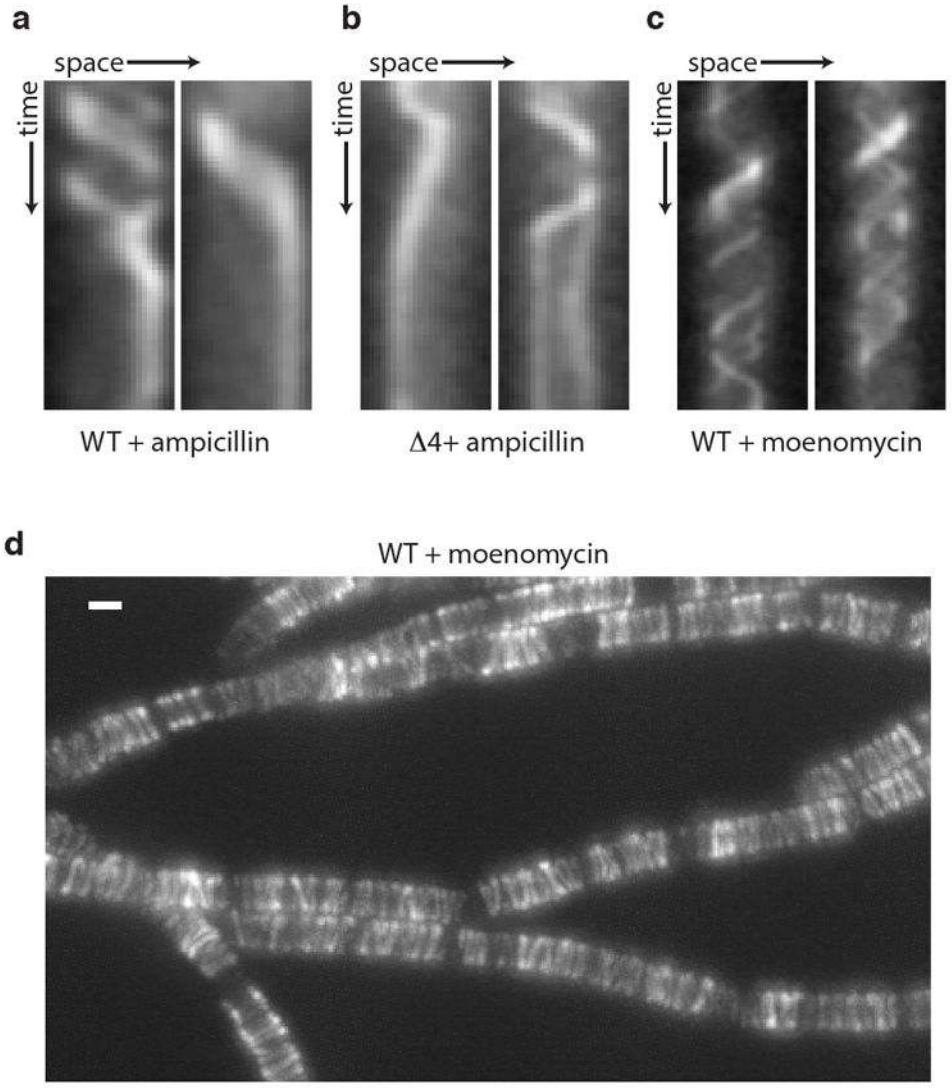

Extended Data Fig. 1. Rod complex dynamics in the presence of different antibiotics

Representative kymographs showing cessation of GFP-Mbl particle movement in **a**, wild-type and **b**, the quadruple (Δ4) aPBP mutant upon treatment with 10 μg/mL ampicillin. **c**, Rod complex motion is unaffected by moenomycin treatment. Cells harboring GFP-Mbl were pre-treated with 1 μg/mL moenomycin for 15 min then imaged in the presence of moenomycin. Representative kymographs of individual GFP-Mbl particles are shown. **(d)** Maximum intensity projection of the timelapse in Supplementary Video 5. Scale bar indicates 1 μm. Data are representative of 3 biological replicates.

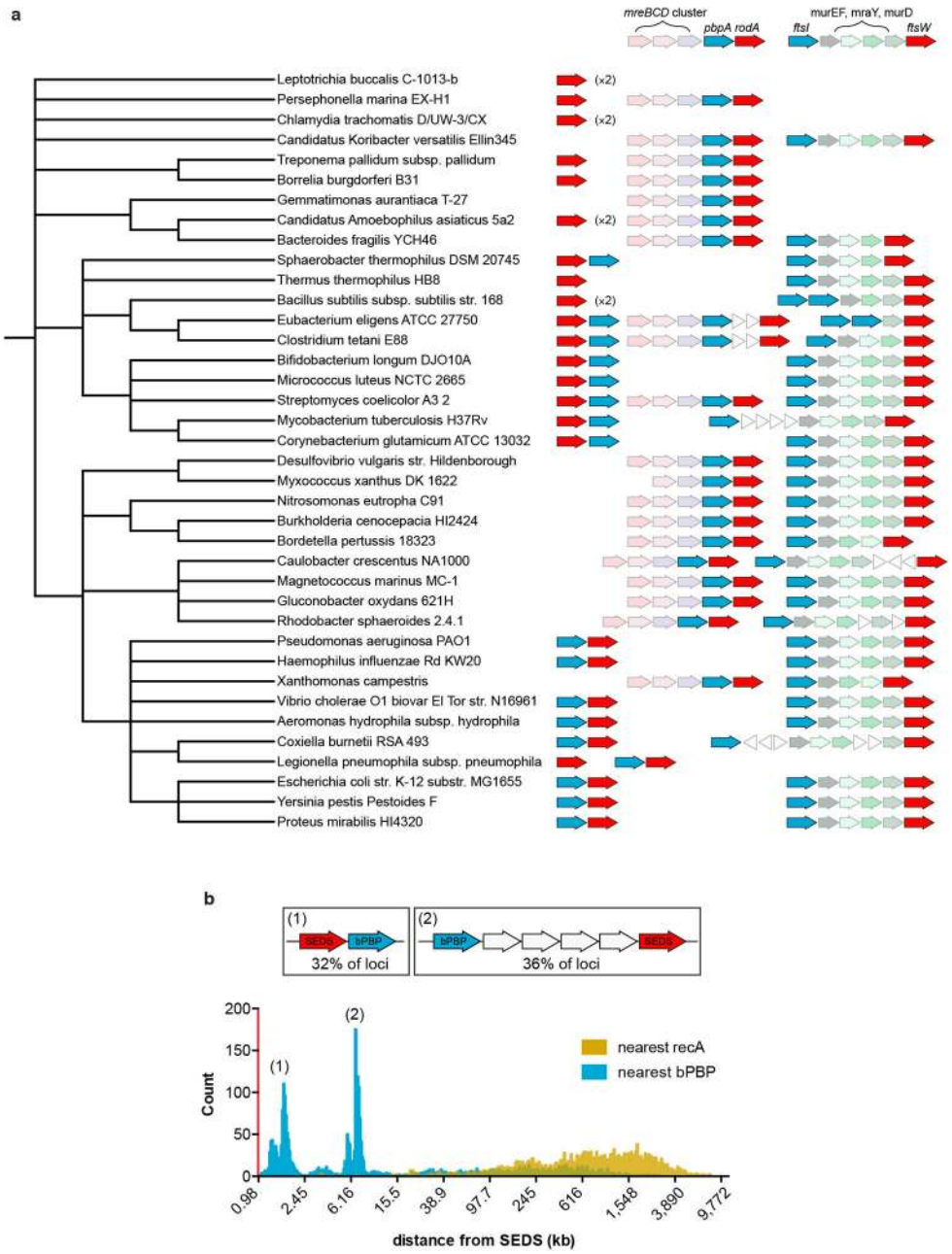

Extended Data Fig. 2. Conserved neighborhood architecture for loci encoding SEDS proteins and bPBPs

a, Diagrams depicting the genomic context of genes encoding SEDS proteins (red) in a diverse set of bacterial taxa. Genes encoding bPBPs are depicted in blue and are frequently located adjacent to SEDS loci. These SEDS-bPBP pairs are often found in the context of the *mreBCD* operon (faded pink), suggesting that these orthologs function in cell elongation. SEDS and bPBP loci are also frequently present in the cluster of cell wall synthesis and cell division genes exemplified by the *E. coli dcw* cluster (faded green) and these orthologs likely function in cell division. Unrelated genes are shown as white triangles. Phylogenetic tree was constructed in PhyLoT (phylot.biobyte.de) and visualized in iToL (itol.embl.de). **b**,

Histogram showing the genetic distance (on $\log_{10}$ scale) between 2,958 SEDS loci (red) and the nearest bPBP locus (blue). Two commonly observed SEDS-bPBP neighborhood architectures are depicted. Distances between SEDS and the nearest *recA* gene are shown in yellow as a negative control. SEDS and bPBP loci were identified using tblastn with five diverse members of each family used as the query.

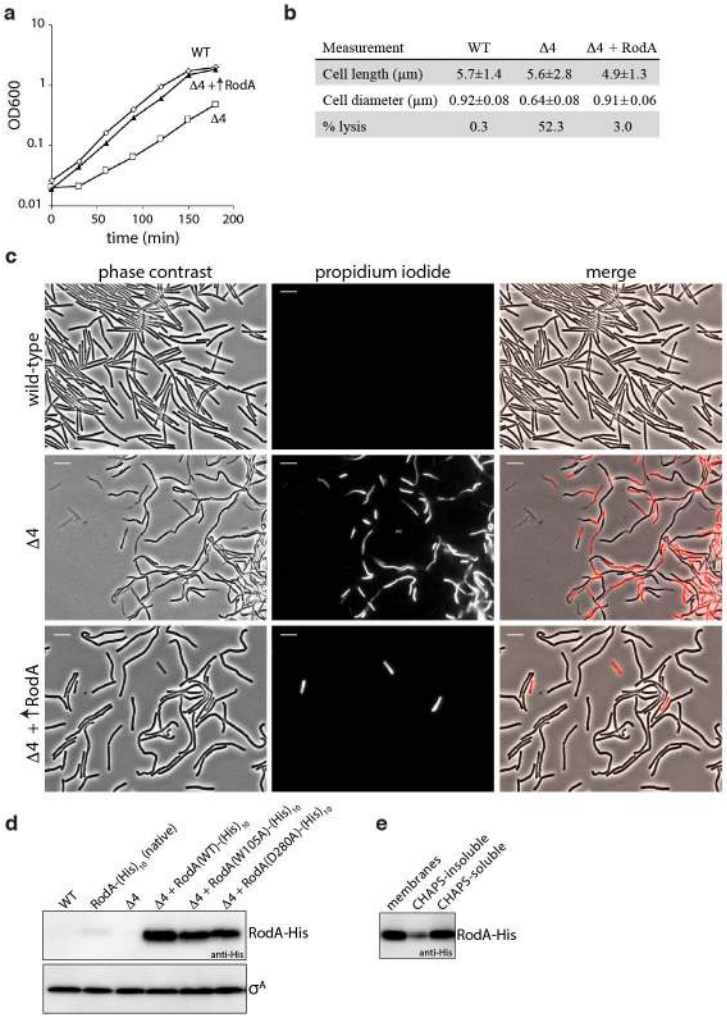

Extended Data Fig. 3. RodA overexpression partially suppresses the phenotypes of the quadruple aPBP mutant

a, Growth curves of wild-type (WT), the quadruple (Δ4) aPBP mutant, and the Δ4 mutant overexpressing *rodA-his10*, representative of three biological replicates. **b**, Quantification of indicated cytological phenotypes, n=500. Error bars denote s.e.m. **c**, Live-dead (propidium iodide) staining of strains analyzed in **a**. Dead cells or cells with membrane integrity defects were visualized by fluorescence microscopy. Images representative of 3 biological replicates. Scale bar indicates 5 μm. **d**, Immunoblot analysis of RodA-His10 levels for the three strains in **a** as well as the Δ4 strain overexpressing nonfunctional mutants W105A and D280A. A fusion of *his10* to *rodA* at its native locus was used to assess wild-type RodA levels (lane 2). Sigma A (σ^A) levels are shown to control for loading. **e**, Detergent

solubilization of RodA-His10 from *B. subtilis* membranes using CHAPS. Anti-His immunoblot showing the relative amounts of solubilized RodA-His10 after overnight incubation with 2% CHAPS and ultracentrifugation at 100,000*g*.

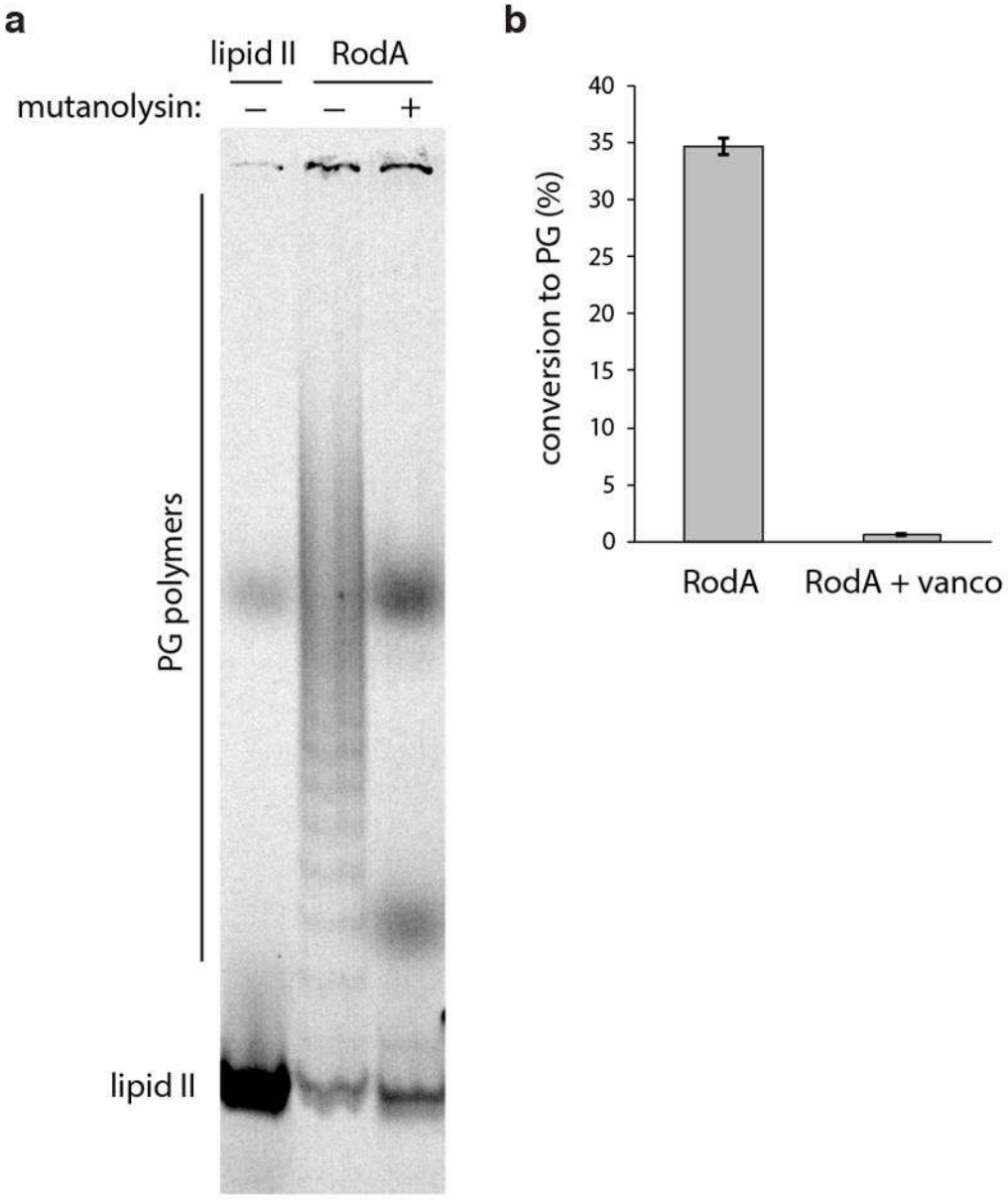

Extended Data Fig. 4. Polymers synthesized by RodA in vitro are susceptible to muramidase digestion

a, To determine whether the products of RodA activity are glycan strands, their susceptibility to cleavage by the muramidase mutanolysin was investigated. Mutanolysin specifically cleaves the β(1,4) linkage between *N*-acetylmuramic acid and *N*-acetylglucosamine in PG glycan chains. 0.2 μM FLAG-RodA was incubated with 4 μM synthetic lipid II for 1 h, then quenched by boiling for 2 min. The products were subjected to overnight digestion with mutanolysin (0.1 mg/ml) at 37°C, and analyzed by SDS-PAGE.

Lipid II, and undigested RodA products are shown for comparison. Data representative of two technical replicates. **b**, The reaction catalyzed by RodA can be inhibited by vancomycin (50 μg/mL), which binds and sequesters the lipid II substrate. Graph denotes the mean from 3 technical replicates, error bars show s.e.m.

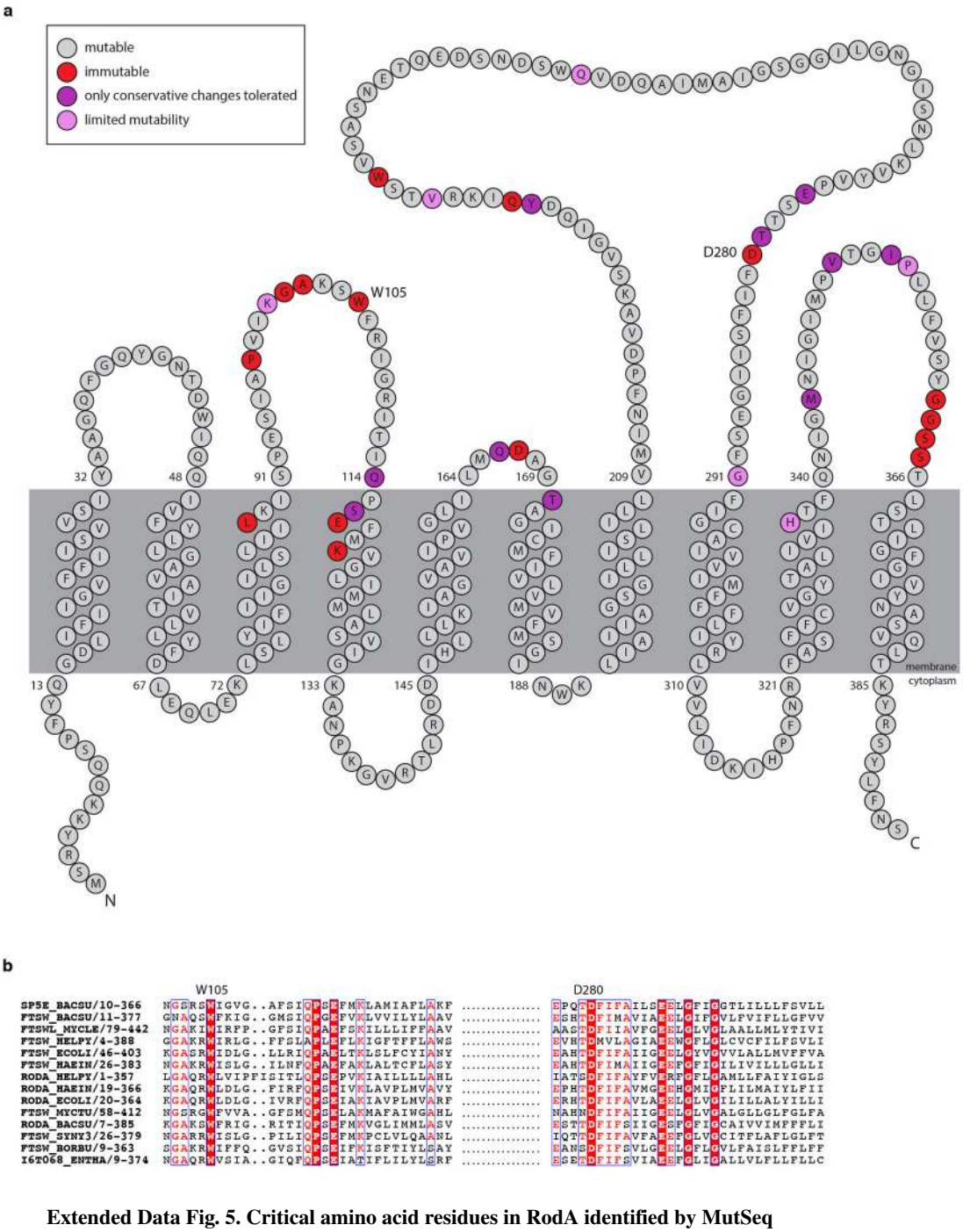

Extended Data Fig. 5. Critical amino acid residues in RodA identified by MutSeq

a, Topological map of the RodA protein. The extent to which each amino acid residue tolerated mutations based on the MutSeq screen are indicated. Residues that tolerated a

spectrum of amino acid changes are shown in grey. Residues that did not tolerate any mutations are shown in red. Residues that only tolerated conservative changes (conservation of charge, hydrophobicity, or functional groups) are in purple. Residues that had limited mutability but tolerated a nonconservative substitution are shown in pink. The complete dataset can be found in Supplementary Table 1. **b**, Multiple sequence alignment (created using ESPRIPT: http://espript.ibcp.fr/) of 14 diverse SEDS proteins with W105 and D280 residues highlighted.

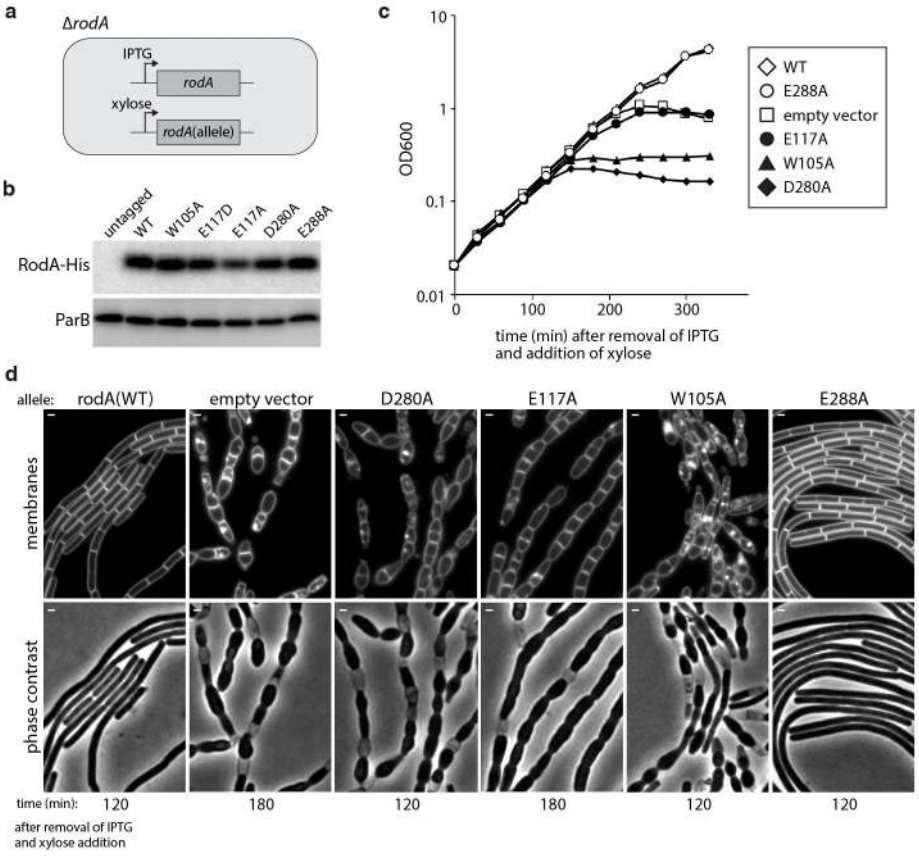

Extended Data Fig. 6. Validation of critical amino acids identified in the MutSeq screen

a, Schematic of the strain used to test a subset of critical amino acid residues in *rodA* identified by MutSeq. A wild-type copy of *rodA* was placed under IPTG-inducible control at an ectopic chromosomal locus (*ycgO*) and the native copy of *rodA* was deleted. The mutant alleles to be tested were placed under xylose-inducible control at a second ectopic locus (*amyE*). As a positive control, a wild-type allele under xylose control was integrated at the second locus. The empty vector was used as a negative control. **b**, Immunoblot analysis of the RodA mutants expressed as His10-tagged fusions under xylose-inducible control, representative of two biological replicates. ParB levels are shown to control for loading. **c**, Growth curves of strains expressing mutant *rodA* alleles. Each strain was grown at 37°C in CH medium in the presence of 500 μM IPTG to maintain expression of wild-type *rodA*. Cultures were then washed three times in medium lacking inducer, diluted to OD600 = 0.02 in CH medium with 10mM xylose, and growth was monitored. Growth curves are

representative of 2 biological replicates. **d**, Morphological phenotypes of the strains analyzed in (c) were examined by fluorescence microscopy at the indicated time points (below the images) after resuspension in xylose-containing medium. Fluorescent images of cell membranes stained with TMA-DPH and phase contrast images are shown. A mutation in the highly conserved residue E288 that was found to be mutable by Mutseq was included as a negative control. Consistent with the Mutseq analysis, substitution to alanine (E288A) supported wild-type growth rates and had no impact on cell morphology.

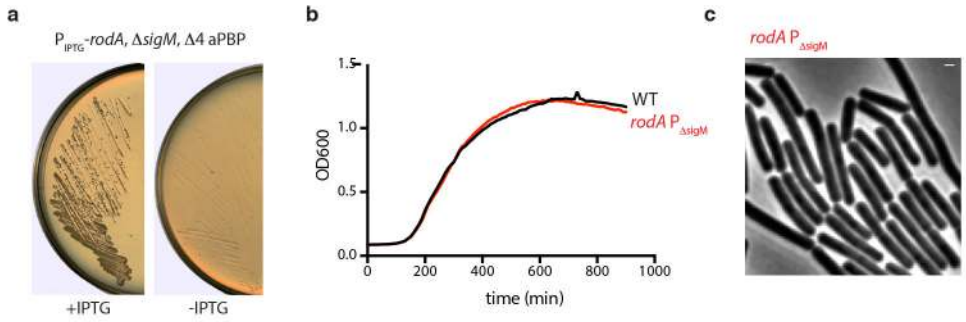

Extended Data Fig. 7. RodA overexpression suppresses the synthetic lethality of Δ*sigM* and the quadruple aPBP mutant

a, LB agar plates onto which a Δ*sigM* Δ4 aPBP strain harboring an IPTG-inducible allele of *rodA* was streaked in the presence and absence of 15 μM IPTG and incubated at 37°C overnight. **b**, The *rodA* allele containing mutations in its SigM-dependent promoter (*rodA* ΔP_{sigM}) grows in a manner indistinguishable from wild-type in the absence of moenomycin. Wild-type (WT) and the *rodA* ΔP_{sigM} mutant were grown in LB and OD600 was monitored continuously. **c**, The *rodA* ΔP_{sigM} mutant has a normal rod-shaped morphology. Phase contrast image of cells harboring the *rodA* ΔP_{sigM} promoter mutant grown to mid-exponential phase in LB medium. All data representative of two biological replicates. Scale bar indicates 1 μm.

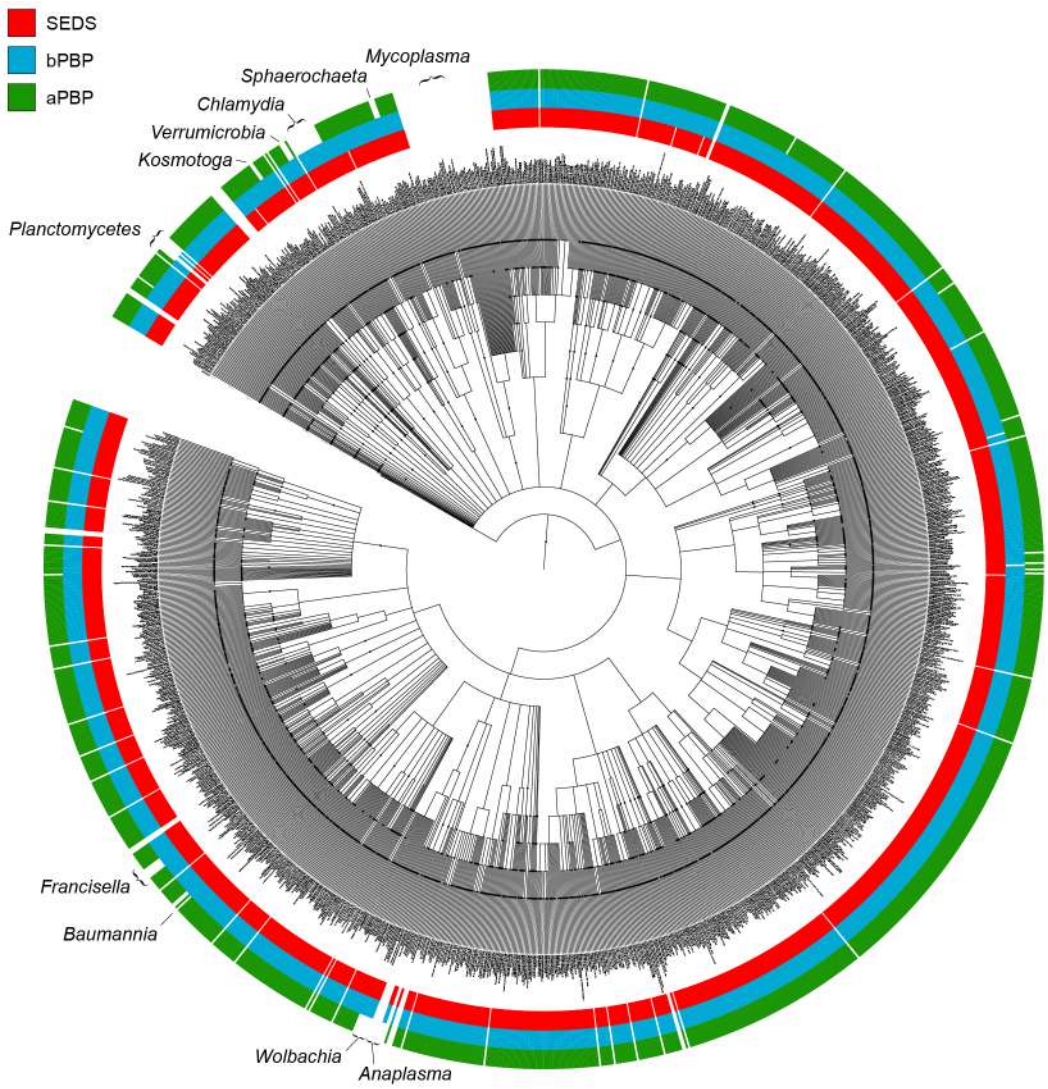

Extended Data Fig. 8. SEDS proteins and bPBPs are more widely conserved than aPBPs

Phylogenetic tree showing distribution of SEDS proteins, bPBPs, and aPBPs in a diverse set of 1773 bacterial taxa. The amino acid sequences of five members of each family were used as queries in a BLASTp search against the NCBI nr database with an E-value cutoff of 10^{-4}. The phylogenetic tree was constructed using PhyloT (phylot.bio-byte.de) and BLASTp results were plotted against the tree. The occurrence of a SEDS protein is indicated in red, a bPBP in blue, and an aPBP in green. The tree was visualized and annotated using iToL (itol.embl.de). Clades whose genomes contain a SEDS protein and bPBP but lack aPBPs are indicated. The PG-less *Mycoplasma* lack all three proteins.

Supplementary Material

Refer to Web version on PubMed Central for supplementary material.

Acknowledgments

We thank past and present members of the Rudner and Bernhardt super group for advice and encouragement, members of the Walker and Kahne labs for help with PGT assays, Deborah Perlstein for initial characterization of a PGT activity in the aPBP quadruple mutant, and Xindan Wang for plasmids. Support for this work comes from the National Institute of Health Grants GM073831 (DZR), RC2 GM092616 (DZR), AI083365 (TGB), AI099144 (TGB and SW), and Center for Excellence in Translational Research (U19 AI109764) (DZR, TGB, SW, DK, JJM).

References

1. Goffin C, Ghuysen JM. Multimodular penicillin-binding proteins: an enigmatic family of orthologs and paralogs. Microbiol Mol Biol Rev. 1998; 62:1079–1093. [PubMed: 9841666]
2. Lombard V, Golaconda Ramulu H, Drula E, Coutinho PM, Henrissat B. The carbohydrate-active enzymes database (CAZy) in 2013. Nucleic Acids Research. 2013; 42:D490–D495. [PubMed: 24270786]
3. Matteï PJ, Neves D, Dessen A. Bridging cell wall biosynthesis and bacterial morphogenesis. Current Opinion in Structural Biology. 2010; 20:749–755. [PubMed: 21030247]
4. Packiam M, Weinrick B, Jacobs WR Jr, Maurelli AT. Structural characterization of muropeptides from *Chlamydia trachomatis* peptidoglycan by mass spectrometry resolves 'chlamydial anomaly'. Proc Natl Acad Sci USA. 2015; 112:11660–11665. [PubMed: 26290580]
5. McPherson DC, Popham DL. Peptidoglycan Synthesis in the Absence of Class A Penicillin-Binding Proteins in *Bacillus subtilis*. Journal of Bacteriology. 2003; 185:1423–1431. [PubMed: 12562814]
6. Arbeloa A, et al. Role of Class A Penicillin-Binding Proteins in PBP5-Mediated β-Lactam Resistance in *Enterococcus faecalis*. Journal of Bacteriology. 2004; 186:1221–1228. [PubMed: 14973044]
7. Rice LB, et al. Role of Class A Penicillin-Binding Proteins in the Expression of β-Lactam Resistance in *Enterococcus faecium*. Journal of Bacteriology. 2009; 191:3649–3656. [PubMed: 19304851]
8. Garner EC, et al. Coupled, Circumferential Motions of the Cell Wall Synthesis Machinery and MreB Filaments in *B. subtilis*. Science. 2011; 333:222–225. [PubMed: 21636745]
9. Domínguez-Escobar J, et al. Processive movement of MreB-associated cell wall biosynthetic complexes in bacteria. Science. 2011; 333:225–228. [PubMed: 21636744]
10. van Teefelen S, et al. The bacterial actin MreB rotates, and rotation depends on cell-wall assembly. Proc Natl Acad Sci USA. 2011; 108:15822–15827. [PubMed: 21903929]
11. Ruiz N. Lipid Flippases for Bacterial Peptidoglycan Biosynthesis. LPI. 2016; 8:21–31.
12. Mercer KLN, Weiss DS. The *Escherichia coli* Cell Division Protein FtsW Is Required To Recruit Its Cognate Transpeptidase, FtsI (PBP3), to the Division Site. Journal of Bacteriology. 2002; 184:904–912. [PubMed: 11807049]
13. Goehring NW, Gonzalez MD, Beckwith J. Premature targeting of cell division proteins to midcell reveals hierarchies of protein interactions involved in divisome assembly. Molecular Microbiology. 2006; 61:33–45. [PubMed: 16824093]
14. Fay A, Meyer P, Dworkin J. Interactions between late-acting proteins required for peptidoglycan synthesis during sporulation. Journal of Molecular Biology. 2010; 399:547–561. [PubMed: 20417640]
15. Fraipont C, et al. The integral membrane FtsW protein and peptidoglycan synthase PBP3 form a subcomplex in *Escherichia coli*. Microbiology. 2010; 157:251–259. [PubMed: 20847002]
16. Wei Y, Havasy T, McPherson DC, Popham DL. Rod shape determination by the *Bacillus subtilis* class B penicillin-binding proteins encoded by *pbpA* and *pbpH*. Journal of Bacteriology. 2003; 185:4717–4726. [PubMed: 12896990]
17. Henriques AO, Glaser P, Piggot PJ, Moran CP. Control of cell shape and elongation by the *rodA* gene in *Bacillus subtilis*. Molecular Microbiology. 1998; 28:235–247. [PubMed: 9622350]
18. Daniel RA, Williams AM, Errington J. A complex four-gene operon containing essential cell division gene *pbpB* in *Bacillus subtilis*. Journal of Bacteriology. 1996; 178:2343–2350. [PubMed: 8636036]

19. Gamba P, Veening JW, Saunders NJ, Hamoen LW, Daniel RA. Two-step assembly dynamics of the *Bacillus subtilis* divisome. Journal of Bacteriology. 2009; 191:4186–4194. [PubMed: 19429628]
20. Ishino F, et al. Peptidoglycan synthetic activities in membranes of *Escherichia coli* caused by overproduction of penicillin-binding protein 2 and rodA protein. Journal of Biological Chemistry. 1986
21. Soding J. Protein homology detection by HMM-HMM comparison. Bioinformatics. 2005; 21:951–960. [PubMed: 15531603]
22. Schmidt G, Mannel D, Mayer H, Whang HY, Neter E. Role of a lipopolysaccharide gene for immunogenicity of the enterobacterial common antigen. Journal of Bacteriology. 1976; 126:579–586. [PubMed: 57114]
23. Wilkinson RG, Gemski P, Stocker BAD. Non-smooth Mutants of *Salmonella typhimurium*: Differentiation by Phage Sensitivity and Genetic Mapping. Journal of General Microbiology. 1972; 70:527–554. [PubMed: 4556257]
24. Telenti A, et al. The *emb* operon, a gene cluster of *Mycobacterium tuberculosis* involved in resistance to ethambutol. Nat Med. 1997; 3:567–570. [PubMed: 9142129]
25. Lizak C, Gerber S, Numao S, Aebi M, Locher KP. X-ray structure of a bacterial oligosaccharyltransferase. Nature. 2011; 474:350–355. [PubMed: 21677752]
26. Kus JV, et al. Modification of Pseudomonas aeruginosa Pa5196 Type IV Pilins at Multiple Sites with D-Araf by a Novel GT-C Family Arabinosyltransferase, TfpW. Journal of Bacteriology. 2008; 190:7464–7478. [PubMed: 18805982]
27. Ye XY, et al. Better substrates for bacterial transglycosylases. J Am Chem Soc. 2001; 123:3155–3156. [PubMed: 11457035]
28. Gampe CM, Tsukamoto H, Wang TSA, Walker S, Kahne D. Modular synthesis of diphospholipid oligosaccharide fragments of the bacterial cell wall and their use to study the mechanism of moenomycin and other antibiotics. Tetrahedron. 2011; 67:9771–9778. [PubMed: 22505780]
29. Robins WP, Faruque SM, Mekalanos JJ. Coupling mutagenesis and parallel deep sequencing to probe essential residues in a genome or gene. Proc Natl Acad Sci USA. 2013; 110:E848–57. [PubMed: 23401533]
30. Mascher T, Hachmann AB, Helmann JD. Regulatory Overlap and Functional Redundancy among *Bacillus subtilis* Extracytoplasmic Function Factors. Journal of Bacteriology. 2007; 189:6919–6927. [PubMed: 17675383]
31. Salzberg LI, Luo Y, Hachmann AB, Mascher T, Helmann JD. The *Bacillus subtilis* GntR Family Repressor YtrA Responds to Cell Wall Antibiotics. Journal of Bacteriology. 2011; 193:5793–5801. [PubMed: 21856850]
32. Liechti GW, et al. A new metabolic cell-wall labelling method reveals peptidoglycan in *Chlamydia trachomatis*. Nature. 2013; 506:507–510. [PubMed: 24336210]
33. Pilhofer M, et al. Discovery of chlamydial peptidoglycan reveals bacteria with murein sacculi but without FtsZ. Nat Comms. 2013; 4
34. van Teeseling MCF, et al. Anammox Planctomycetes have a peptidoglycan cell wall. Nat Comms. 2015; 6:6878.
35. Jeske O, et al. Planctomycetes do possess a peptidoglycan cell wall. Nat Comms. 2015; 6:7116.
36. Vollmer J, et al. Requirement of lipid II biosynthesis for cell division in cell wall-less *Wolbachia*, endobacteria of arthropods and filarial nematodes. International Journal of Medical Microbiology. 2013; 303:140–149. [PubMed: 23517690]
37. Sham LT, et al. Bacterial cell wall. MurJ is the flippase of lipid-linked precursors for peptidoglycan biogenesis. Science. 2014; 345:220–222. [PubMed: 25013077]
38. Meeske AJ, et al. MurJ and a novel lipid II flippase are required for cell wall biogenesis in *Bacillus subtilis*. Proc Natl Acad Sci USA. 2015; 112:6437–6442. [PubMed: 25918422]
39. Vasudevan P, McElligott J, Attkisson C, Betteken M, Popham DL. Homologues of the *Bacillus subtilis* SpoVB Protein Are Involved in Cell Wall Metabolism. Journal of Bacteriology. 2009; 191:6012–6019. [PubMed: 19648239]
40. Vasudevan P, Weaver A, Reichert ED, Linnstaedt SD, Popham DL. Spore cortex formation in *Bacillus subtilis* is regulated by accumulation of peptidoglycan precursors under the control of sigma K. Molecular Microbiology. 2007; 65:1582–1594. [PubMed: 17714441]

41. Gibson DG, et al. Enzymatic assembly of DNA molecules up to several hundred kilobases. Nature Methods. 2009; 6:343–345. [PubMed: 19363495]

42. Adachi M, et al. Degradation and Reconstruction of Moenomycin A and Derivatives: Dissecting the Function of the Isoprenoid Chain. J Am Chem Soc. 2006; 128:14012–14013. [PubMed: 17061868]

43. Fujita M. Temporal and selective association of multiple sigma factors with RNA polymerase during sporulation in *Bacillus subtilis*. Genes Cells. 2000; 5:79–88. [PubMed: 10672039]

44. Lin DC, Levin PA, Grossman AD. Bipolar localization of a chromosome partition protein in *Bacillus subtilis*. Proc Nat Acad Sci. 1997; 94:4721–4726. [PubMed: 9114058]

45. Kruse AC, et al. Structure and dynamics of the M3 muscarinic acetylcholine receptor. Nature. 2012; 482:552–556. [PubMed: 22358844]

46. Eiamphungporn W, Helmann JD. The *Bacillus subtilis* σM regulon and its contribution to cell envelope stress responses. Molecular Microbiology. 2008; 67:830–848. [PubMed: 18179421]

47. Baba T, et al. Construction of *Escherichia coli* K-12 in-frame, single-gene knockout mutants: the Keio collection. Mol Syst Biol. 2006; 2

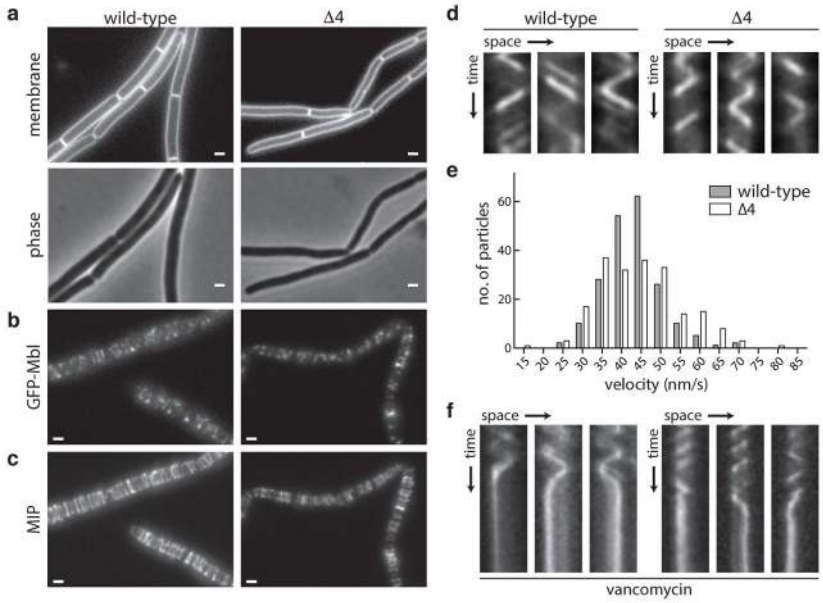

Fig. 1. The Rod complex is functional in the absence of all known PG polymerases

a, Morphological defects of *B. subtilis* cells lacking all four aPBPs. **b–e**, Dynamics of the Rod complex component Mbl (GFP-Mbl) in the presence and absence of the aPBPs (Δ4). **b**, Snapshots and **c**, maximum intensity projections (MIP) from timelapse microscopy. **d**, Kymographs showing the motion of individual GFP-Mbl particles over time. **e**, Histogram of particle velocities, n=200. **f**, Kymographs of GFP-Mbl particles upon vancomycin treatment. Data are representative of four biological replicates. Scale bars indicate 1 μm.

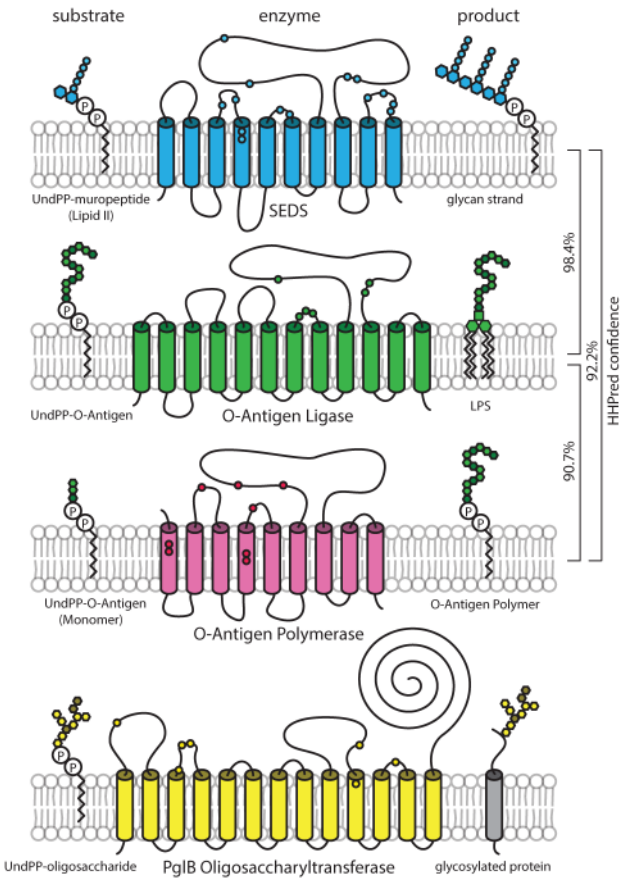

Fig. 2. The SEDS proteins bear similarity to known glycosyltransferases

Schematic diagrams of the SEDS protein RodA and known glycosyltransferases from gram-negative bacteria with their undecaprenyl pyrophosphate-linked substrates and products. In blue, RodA from *B. subtilis* is shown alongside its putative substrate and product, undecaprenyl pyrophosphate-linked precursor (Lipid II) and glycan strands, respectively. O-antigen ligase WaaL (green), O-antigen polymerase Wzy (pink) and N-linked oligosaccharyltransferase PglB (yellow) are shown. Biochemical and genetic analyses indicate that functionally important residues are located in the periplasmic loops, shown schematically as small circles. Similarity between protein families detected by HHpred is indicated.

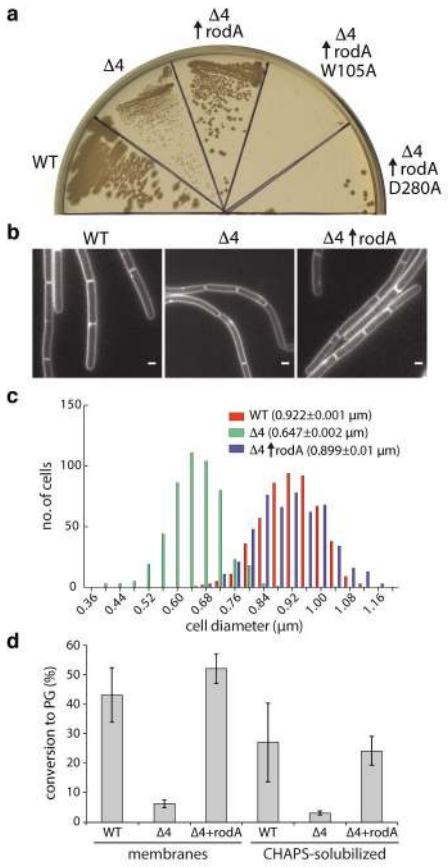

Fig. 3. RodA overexpression partially suppresses the phenotypes of the aPBP mutant

a, Suppression of growth defects and **b**, morphological defects in the Δ4 mutant by *rodA* overexpression, representative of 3 biological replicates. Scale bar indicates 1 μm. **c**, Histogram of cell diameters for the indicated strains, n=500. Average diameter is indicated in parenthesis. **d**, PGT activity catalyzed by membranes and CHAPS-solubilized membrane proteins derived from the indicated strains. Data show the mean of 3 biological replicates, error bars denote standard error of the mean (s.e.m.).

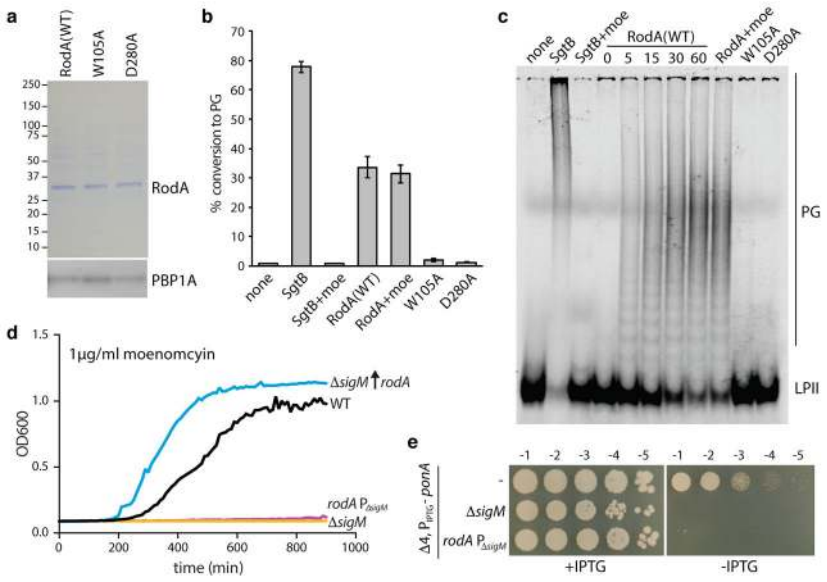

Fig. 4. RodA has glycosyltransferase activity in vitro

a, Purified FLAG-RodA and point mutants, and corresponding anti-PBP1A immunoblot. **b**, PGT activity of purified proteins and positive control SgtB in the presence and absence of moenomycin (moe). Error bars indicate s.e.m. from 2 technical and 2 biological replicates. **c**, SDS-PAGE of reactions from **b**, analyzed after 60 min or as indicated (in minutes). **d** and **e**, RodA induction is necessary and sufficient for growth in the absence of aPBPs. Representatives from 3 biological replicates. **d**, Moenomycin inhibition and **e**, depletion of *ponA* (encoding the major aPBP) in the indicated strains.